3D Vertically Aligned Li Metal Anodes with Ultrahigh Cycling Currents and Capacities of 10 mA cm^{-2}/20 mAh cm^{-2} Realized by Selective Nucleation within Microchannel Walls

Xuejie Gao, Xiaofei Yang, Keegan Adair, Xiaona Li, Jianwen Liang, Qian Sun, Yang Zhao, Ruing Li, Tsun-Kong Sham,* and Xueliang Sun*

Although metallic lithium is regarded as the "Holy Grail" for next-generation rechargeable batteries due to its high theoretical capacity and low overpotential, the uncontrollable Li dendrite growth, especially under high current densities and deep plating/striping, has inhibited its practical application. Herein, a 3D-printed, vertically aligned Li anode (3DP-VALi) is shown to efficiently guide Li deposition via a "nucleation within microchannel walls" process, enabling a high-performance, dendrite-free Li anode. Moreover, the microchannels within the microwalls are beneficial for promoting fast Li$^+$ diffusion, supplying large space for the accommodation of Li during the plating/stripping process. The high-surface-area 3D anode design enables high operating current densities and high areal capacities. As a result, the Li–Li symmetric cells using 3DP-VALi demonstrate excellent electrochemical performances as high as 10 mA cm^{-2}/10 mAh cm^{-2} for 1500 h and 5 mA cm^{-2}/20 mAh cm^{-2} for 400 h, respectively. Additionally, the Li–S and Li–LiFePO$_4$ cells using 3DP-VALi anodes present excellent cycling stability up to 250 and 800 cycles at a rate of 1 C, respectively. It is believed that these new findings could open a new window for dendrite-free metal anode design and pave the way toward energy storage devices with high energy/power density.

1. Introduction

Given their high specific capacity and high discharge voltage, Li metal batteries (LMBs) have the potential to achieve energy densities over 500 Wh kg^{-1} when combined with S and O$_2$ cathodes, which is 2–3 times that of state-of-the-art Li-ion batteries.[1] Nevertheless, the nonuniform Li deposition during the plating/stripping process is still a significant challenge that slows down the progress of practical LMBs. The uncontrolled deposition and Li dendrite growth induce continuous consumption of electrolyte and formation of unstable solid electrolyte interphase (SEI) components, eventually leading to internal short circuits and poor electrochemical performance.[2]

Many strategies such as the introduction of protection layers,[3] in situ formation of SEI components,[4] guided Li nucleation,[5] control of Li salt concentration,[6] Li morphology control,[7,8] and application of solid-state-electrolytes (SSEs)[9] have been demonstrated to be effective in eliminating the aforementioned problems of the Li metal anode. Despite the great achievements made to date, the poor ionic conductivities of most protection layers, continuous consumption of electrolyte additives, and large SSE/electrode interfacial resistance significantly limit the practical use of conventional Li anodes to low current densities and areal capacities.

Recently, the fabricating 3D Li anodes by electrochemical deposition, molten Li infusion, and mechanical pressurization has received increasing attention toward achieving high-energy/power density LMBs.[10] On one hand, the 3D Li anode can provide a large specific surface for reducing local current density and facilitating smooth Li deposition. On the other hand, the entrapped voids in the 3D Li anode supplies a large storage space for Li accommodation.[10a,c] A fly in the ointment is that the Li growth directions are random because of lacking selectivity, increasing the risk of dendrites penetrating the separator, especially operating at high current densities and high areal capacities.[11] Very recently, Zhang's group developed a simple rolling-cutting/coiling method by rolling the closed tight separator (PE or glass fiber) and Li foil into a Swiss roll shape.[12] It shows the top-side Li presented the highest current density distribution, resulting in a selective "side deposition-dissolution" process, which significantly lowered the risk of internal short-circuiting. The results showed that the unique 3D Li structure can tolerate a high current density of over 5 mA cm^{-2}. However, limited by the space/specific surface based on the millimeter-scale structure, the cells can run for less than 200 h even within a low areal capacity of 1 mAh cm^{-2}.

X. Gao, Dr. X. Yang, K. Adair, Dr. X. Li, Dr. J. Liang, Dr. Q. Sun,
Dr. Y. Zhao, R. Li, Prof. X. Sun
Department of Mechanical and Materials Engineering
University of Western Ontario
London, Ontario N6A 5B9, Canada
E-mail: xsun9@uwo.ca
X. Gao, Prof. T.-K. Sham
Department of Chemistry
University of Western Ontario
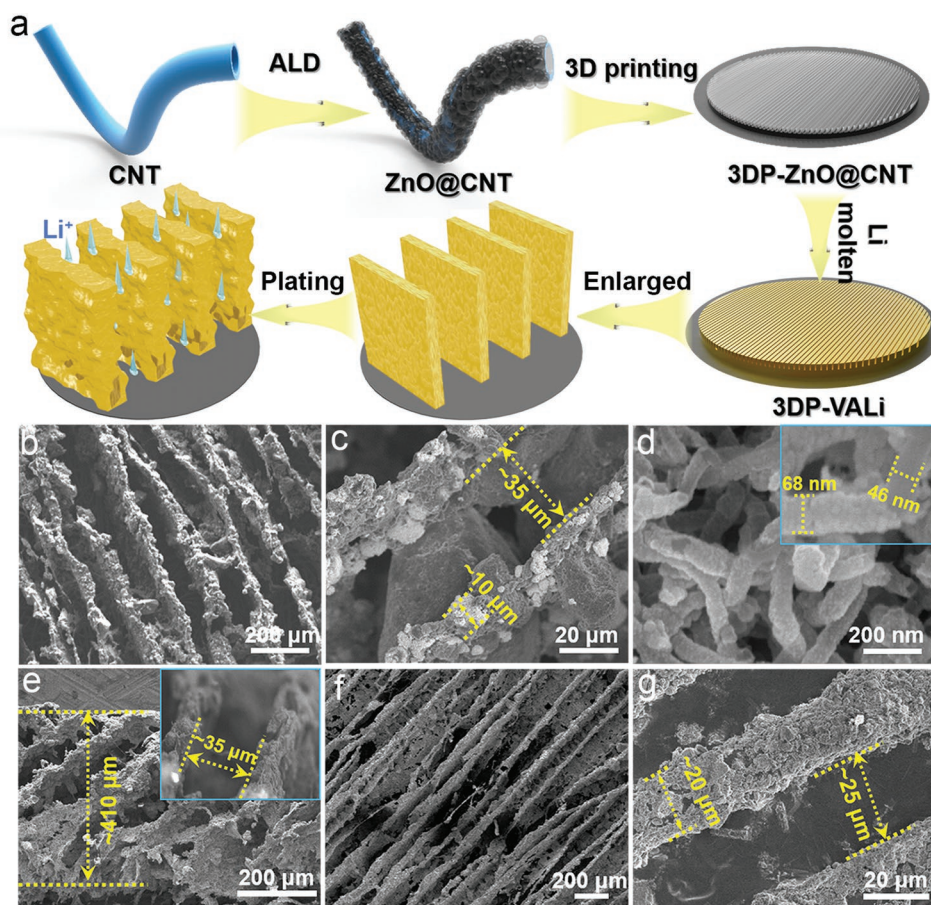London, Ontario N6A 5B7, Canada
E-mail: tsham@uwo.ca

Figure 1. a) Schematic diagram of the 3DP-VALi fabrication process, b–d) top sectional SEM images of 3D-printed CNT@ZnO at different magnifications, e) cross sectional SEM image of CNT@ZnO template, and f,g) SEM images of 3DP-VALi at different magnifications.

There is no doubt that it is not satisfied with the practical application of LMBs. With this in mind, new designs are needed to maximize the advantages of this concept for both long cycling life and high current density/areal capacity Li anodes.

Herein, we developed a 3D printed vertically aligned Li anode (3DP-VALi) with well-controlled microscale features for selective "side deposition," where Li preferably deposits on the microwalls of 3DP-VALi with a lithiophilic ZnO coating. Moreover, the numerous vertically aligned microchannels exist among the microwalls provide a large space for facilitating Li$^+$ transport, accommodating deposited Li as well as alleviating volume change. Based on the microscale structure, selective "nucleation within microchannel walls," the assembled Li–Li symmetric cells achieve an ultralong cycling life of 3000 h at current density/areal capacity of 1 mA cm^{-2}/1 mAh cm^{-2}. More importantly, the Li–Li symmetric cell demonstrates an excellent long cycling life of 1500 and 400 h at ultrahigh current densities/areal capacities of 10 mA cm^{-2}/10 mAh cm^{-2} and 5 mA cm^{-2}/20 mAh cm^{-2}, respectively.

2. Results and Discussion

The 3DP-VALi was produced via combining a 3D printing technique with a freeze-drying method, followed by an infusion of molten Li into the 3D scaffold at a high temperature. As shown in **Figure 1**a, before printing, an amorphous ZnO layer (determined by the X-ray powder diffraction (XRD) pattern in Figure S1 in the Supporting Information) was coated on the surface of carbon nanotube (CNT) via an atomic layer deposition (ALD) method to create a lithiophilic surface. The thickness of ZnO was determined to be around 10 nm (Figure 1d).[13] Afterward, the ZnO@CNT was mixed with an aqueous binder and then printed into controlled dense line patterns on a carbon paper (CP) current collector.[14] To achieve the vertically aligned structured 3D-VALi host, the printed patterns were freeze-dried after printing. Due to the anisotropic crystal growth kinetics, the ice presents a lamellar structure during the freeze-drying process, which applied as the in situ templates to divide the patterns into numerous vertically aligned microwalls (Figure S2, Supporting Information).[15] During the Li plating process, the Li is preferably deposited on the lithiophilic microwalls instead of depositing on the surface of lithiophobic CP current collector, resulting in a "nucleation within microchannel walls" process. According to previous reports, such a unique "side deposition" can significantly lower the risk of internal short-circuiting.[12,16] What's more, those microwalls provide a large specific surface area for Li deposition sites, greatly reducing the local current density. Among the microwalls are vertically aligned microchannels. As shown in Figure 1b,c,e, the microwalls and the

microchannels exhibit thicknesses of 10 and 35 µm, respectively, and the total thickness of the host is 410 µm. Due to the lithophilic property of ZnO, the Li metal is easily infused into the 3D host and the whole Li infusion process only costs 12 s (Figure S3, Supporting Information). After the Li infusion, the morphology of the 3DP-VALi is checked by scanning electron microscope (SEM). As shown in Figure 1f,g, the broadened microwalls from 10 to 20 µm and reduced width of the microchannels from 35 to 25 µm suggest that Li is successfully filled into the 3D structure. Moreover, it is noteworthy that there are some microchannels that are still maintained for Li accommodation, facilitating Li$^+$ transport and alleviating volume change during the plating/stripping process, which helps enhance the cycling life and improve the operating current density/areal capacity as well.

The Li plating/stripping behavior and electrochemical performance of 3DP-VALi is studied though Li–Li symmetrical cells, where bare Li is chosen for comparison. **Figure 2** shows 3DP-VALi and bare Li symmetrical cells in an ether-based electrolyte with 50 µL electrolyte (1 M Li lithium bis(trifluoromethanesulfonyl)imide (LITFSI) in 1,3-dioxolane (DOL)/dimethyl ether (DME) of 1:1 volume ratio with 1 wt% LiNO$_3$). In Figure 2a, with a current density of 1 mA cm^{-2} and a capacity of 1 mAh cm^{-2}, both of the cells exhibit excellent cycling stability in the first 1100 h with overpotentials around 10 mV

(3DP-VALi) and 32 mV (bare Li), respectively. After 1500 h, the overpotential of bare Li increases sharply to over 105 mV, while the 3DP-VALi is able to maintain its cycling stability. Even after 3000 h, the overpotential of 3DP-VALi is only 16 mV with negligible change. Furthermore, the rate capability is studied at various current densities ranging from 0.5 to 10 mA cm^{-2} (half cycling time: 1 h). As shown in Figure 2b, the 3DP-VALi shows lower overpotentials at all current densities, which can be attributed to the large surface area provided by 3DP-VALi that reduces the local current density. The impedance spectroscopy measurements conducted on the symmetric cells illustrate that the 3DP-VALi anode has a significantly smaller resistance compared to bare Li (Figure S4, Supporting Information), which coincides well with the lower polarization observed in the voltage profiles. It should be noted that the 3DP-VALi displays stable plating/stripping behavior, even at an ultrahigh current density of 10 mA cm^{-2} with a relatively low overpotential around 0.4 V. On the contrary, the occurrence of short-circuits is observed in the bare Li cell when the current density increases to 8 mA cm^{-2}, which can be attributed to the nonuniform Li deposition and serious Li dendrite growth at high current densities. It is well known that the cycling life, operating current densities and areal capacities play important roles in the design and development of high energy/power density rechargeable batteries. Accordingly, the plating/stripping behavior of 3DP-VALi
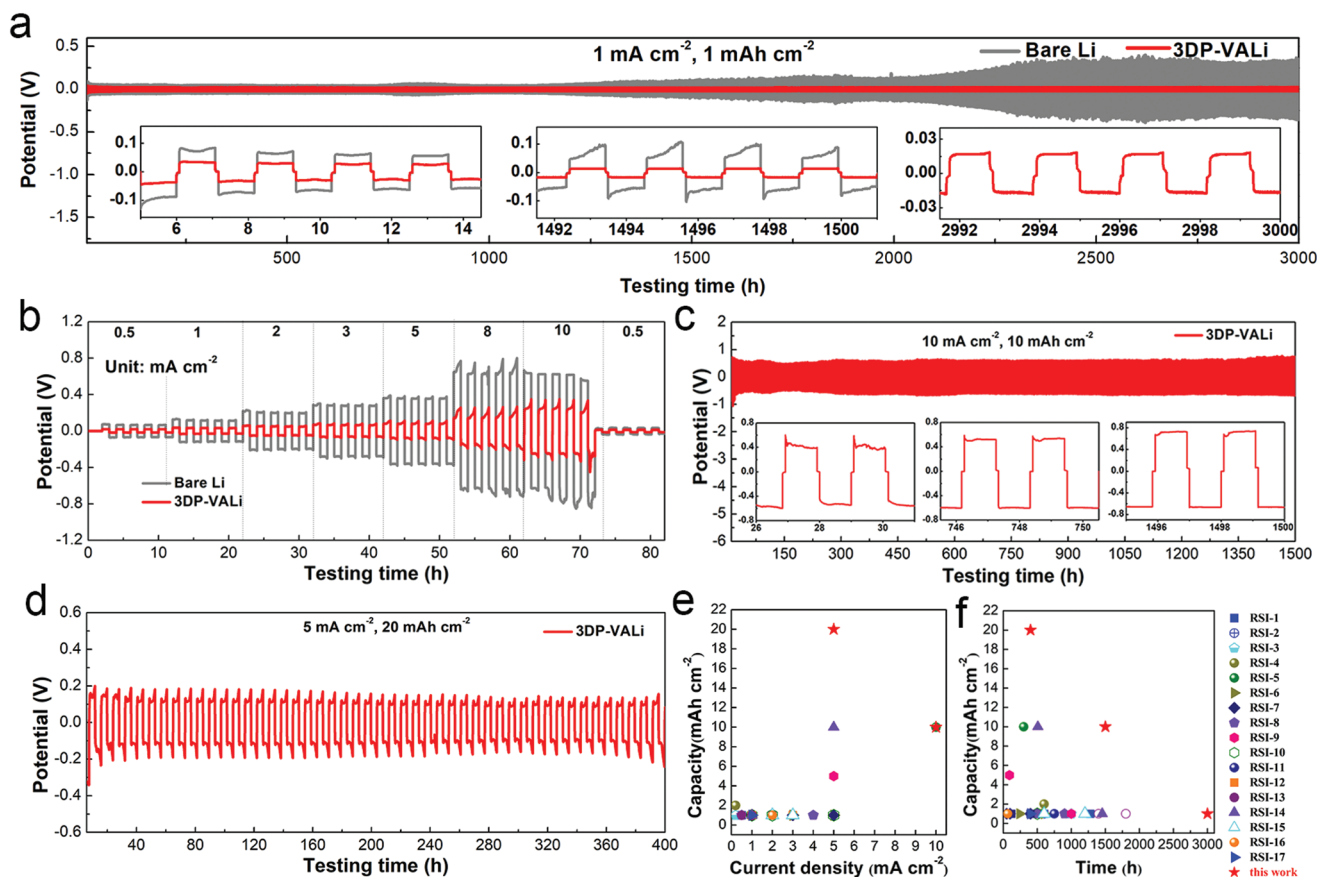

Figure 2. Electrochemical performance of lithium symmetric cells with ether electrolyte. a) 3DP-VALi and bare Li symmetric cells cycled at a current density of 1 mA cm^{-2} and 1 mAh cm^{-2}. b) Rate capability testing with current densities from 0.5 to 10 mA cm^{-2}. Symmetric cell cycling at a current density of c) 10 mA cm^{-2}, 10 mAh cm^{-2}, and d) 5 mA cm^{-2}, 20 mAh cm^{-2}. e,f) Comparison of this work with other lithium symmetric cell from literature.

under elevated current densities (5 and 10 mA cm^{-2}) and areal capacities (10 and 20 mAh cm^{-2}) is explored. Promisingly, the 3DP-VALi anode achieves stable plating/stripping performance at those elevated current densities/areal capacity for 1500 h (10 mA cm^{-2}, 10 mAh cm^{-2}; Figure 2c) and 400 h (5 mA cm^{-2}, 20 mAh cm^{-2}; Figure 2d) with overpotentials of around 710 and 150 mV, respectively. The significantly improved electrochemical performance of Li–Li symmetric cells with 3DP-VALi can be attributed to the "nucleation within microchannel walls" and unique structure of 3DP-VALi that can accommodate the large Li cycling, reducing local current density, alleviate volume change, and suppress the Li dendrite growth. Furthermore, the cycling performance of the 3DP-VALi electrodes are superior to recent publications with respect to cycling life, operating current density, and areal capacity, as shown in Figure 2e,f and Table S1 in the Supporting Information.

To clarify the Li plating/stripping behavior of the 3DP-VALi anode, the surface morphology of the anodes at different stages of cycling is observed by SEM. As illustrated in **Figure 3**a and

displayed in Figure 3c–e, it can be clearly observed that Li is initially deposited on the microwalls of the 3DP-VALi due to the lithiophilic surface, resulting in selective "nucleation within microchannel walls." When the Li plating capacity increases from 1 to 5 mAh cm^{-2}, the microchannels are gradually filled. It is noteworthy that no Li is found on the top surface, which is in agreement well with Cui and Zhang's COMSOL simulations.[11,12] After increasing the plating capacity to 10 mAh cm^{-2}, the microchannels are completely filled (Figure S5a, Supporting Information). In contrast, for the bare Li shown in Figure 3b, there is preferential nucleation at defects, where higher localized current densities are realized, leading to nonuniform Li deposition and undesirable Li dendrite growth. Interestingly, significant differences between the 3DP-VALi and bare Li can also be observed during the stripping process. The Li occupation in the 3DP-VALi porous structure is highly reversible and it can be completely dissolved during the stripping process (Figure 3f; Figure S5b, Supporting Information), which is meant to prolong the cycling life of Li–Li symmetric cells.
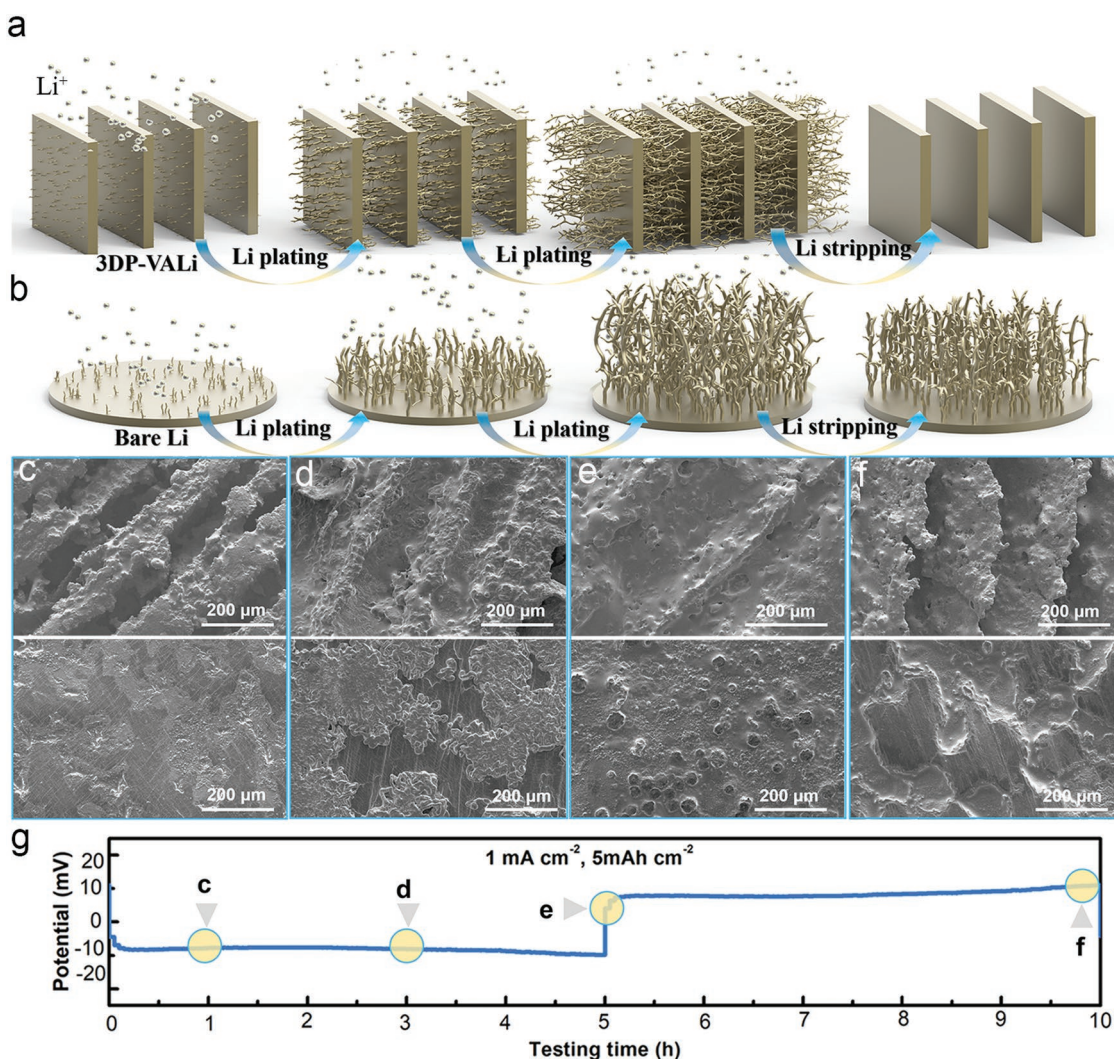

Figure 3. Schematic illustration of the lithium plating and stripping process of a) 3DP-VALi and b) bare Li. SEM images of surface morphology evolution of 3DP-VALi and bare Li anode after c) 1 mAh cm^{-2}, d) 3 mAh cm^{-2}, and e) 5 mAh cm^{-2} of Li deposition, and f) after one plating and stripping cycle after 5 mAh cm^{-2}. g) The voltage profile indicated the Li plating and stripping states at a current density of 1 mA cm^{-2}, corresponding to (c)–(f).

Nevertheless, a highly irreversible stripping process is observed for bare Li. After stripping, a rough surface is obtained and lots of Li pits are observed. The inhomogeneous and irreversible Li plating/stripping process is the main reason for the Li dendrite growth, dead Li formation and limited cycling life of the Li–Li symmetric cells. The differences between the Li plating/stripping process of 3DP-VALi and bare Li further highlights the merits of 3DP-VALi in inhibiting Li dendrite growth and clarifies the improvements of the Li–Li symmetric cell performance.

To further demonstrate the unique properties of the 3DP-VALi, the electrochemical performance of two different energy storage systems using 3DP-VALi and bare Li anodes is investigated.[17] The electrolyte used in full cells test is controlled as around 50 μL for both Li–S and Li-ion batteries. The Li–S coin cells are first tested under galvanostatic charge/discharge current densities in the range of 0.1 to 1 C between 1.7 and 2.8 V, where same ether electrolyte in Li–Li symmetric cells is applied as the electrolyte and sulfur content is determined to be 64 wt% (Figure S8, Supporting Information). As illustrated in **Figure 4**a, the 3DP-VALi-based Li–S cells present better rate-performance compared with bare Li. At a rate of 1 C, the 3DP-VALi-based Li–S cell delivered a high capacity of around 800 mAh g^{-1}, which is higher than its counterpart. The improved C-rate

performance can be attributed to the fast Li$^+$ transport in the microchannels of 3DP-VALi, thus leading to lower resistances and lower overpotentials.[17a] The overpotential of Li–S batteries is determined by the voltage difference based on the median of second discharge plateau at different current densities, according to the previous report.[17b] As displayed by the electrochemical impedance spectroscopy (EIS) results shown in Figure S9 in the Supporting Information, the cell assembled with 3DP-VALi exhibits a low charge transfer resistance (R_{ct}) of 48 Ω, which is 2/3 of that found for the cell using bare Li anode. Under a current density of 1 C, the cell using 3DP-VALi anode delivers a low overpotential about 0.45 V (Figure 4b), whereas that of the cell with bare Li anode is 0.5 V (Figure S10, Supporting Information), indicating the lower energy barrier of Li stripping/plating with 3DP-VALi anode in Li–S batteries. Moreover, the cycling performance of the cells assembled with 3DP-VALi and bare Li anodes are tested under a C-rate of 1 C. As shown in Figure 4c, after fast capacity decay in the first 5 cycles at 0.1 C, the cells using 3DP-VALi and bare Li anodes delivers reversible capacities of around 935 and 580.1 mAh g^{-1} (Figure S11, Supporting Information; operating C-rate: 1 C), respectively. The cell using 3DP-VALi anode displays very stable cycling with a reversible capacity of 756.1 mAh g^{-1} after
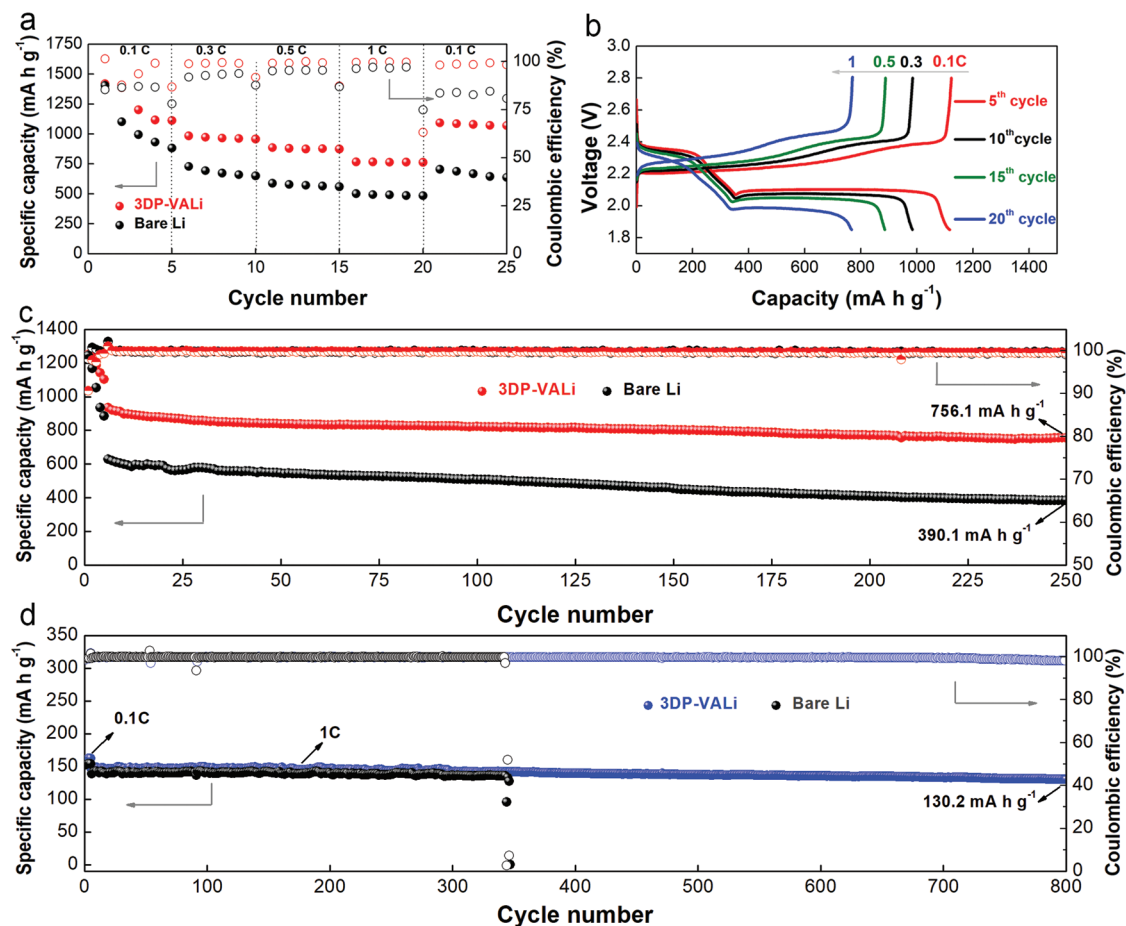

Figure 4. Electrochemical performance of full cells. a) KB@S/3DP-VALi and KB@S/Li rate performance from 0.1 to 1 C (sulfur loading: ≈2.2 mg cm^{-2}). b) Charge and discharge profile of KB@S/3DP-VALi at different rates. c) KB@S/3DP-VALi and KB@S/Li long cycling performance at 1 C. d) LFP/3DP-VALi and LFP/Li cycling performance at 1 C (LFP loading: ≈13.6 mg cm^{-2}).

250 cycles, corresponding to a high capacity retention of ≈81% and a low capacity attenuation of 0.078% per cycle. In comparison, the cell using bare Li anode shows much lower reversible capacity and faster capacity decay, which is 390.1 mAh g^{-1} after cycling. The results further confirm that the 3DP-VALi with its unique "side-deposition" process can remarkably increase the cycle life of the Li anode and improve the reversible capacity and rate-performance of Li–S batteries through enhanced Li$^+$ transport and dead Li/Li dendrite suppression. Moreover, for the carbonate electrolyte system, LiFePO$_4$ (LFP) is chosen as the cathode materials to demonstrate the merits of 3DP-VALi anode. As shown in Figure 4d, in the bare Li-based Li–LFP cell, the cell happens to a short circuit after 340 cycles. Conversely, using 3DP-VALi as the anode, the Li–LFP maintains an extremely stable capacity of around 130.2 mAh g^{-1} after 800 cycles.

3. Conclusion

To conclude, we have developed a 3DP-VALi with well-controlled microscale features for selective "nucleation within microchannel walls," which can successfully suppress Li dendrites. Li preferably nucleates and grows on the surface of the lithiophilic microwalls, where the vertically aligned microchannels are able to facilitate Li$^+$ transport, and further provide large space for Li accommodation. With this in mind, the Li–Li symmetric cells assembled with 3DP-VALi anodes achieve an ultralong cycling life of 3000 h at a current density of 1 mA cm^{-2} with a capacity limit of 1 mAh cm^{-2}. Furthermore, ultrahigh plating/stripping current densities/capacities of 10 mA cm^{-2}/10 mAh cm^{-2} and 5 mA cm^{-2}/20 mAh cm^{-2} are realized with a long cycle life of 1500 and 400 h, respectively. To the best of our knowledge, these results demonstrate the highest areal capacity and cycle life in Li–Li symmetric cell format. We believe that the selective "nucleation within microchannel walls" in the 3D vertically aligned structure with controllable Li growth orientation can effectively suppress the metal dendrites (such as Li), achieving a series of dendrite-free metal anodes and paving the way energy storage devices with high energy/power density.

Supporting Information

Supporting Information is available from the Wiley Online Library or from the author.

Conflict of Interest

The authors declare no conflict of interest.

Author Contributions

X.G. and X.Y. contributed equally to this work. They conceived the idea and designed the experiments. X.S. and T.-K.S. as supervisors gave guidance and discussion to the project. K.A. conducted atomic layer deposition (ALD) coatings for the project. Q.S. helped with the design and discussed the experiments. R.L. assisted with characterizations. X.L. and X.G. did the scanning electron microscope (SEM), and J.L. did the X-ray powder diffraction (XRD) characterization. Y.Z. assisted with the analysis of Li symmetric data. All authors discussed the results and commented on the manuscript.

[1] a) P. G. Bruce, S. A. Freunberger, L. J. Hardwick, J. M. Tarascon, *Nat. Mater.* **2012**, *11*, 19; b) X. Ji, K. T. Lee, L. F. Nazar, *Nat. Mater.* **2009**, *8*, 500; c) X. Yang, X. Li, K. Adair, H. Zhang, X. Sun, *Electrochem. Energy Rev.* **2018**, *1*, 239; d) X. Yang, X. Gao, Q. Sun, S. P. Jand, Y. Yu, Y. Zhao, X. Li, K. Adair, L. Y. Kuo, J. Rohrer, J. Liang, X. Lin, M. N. Banis, Y. Hu, H. Zhang, X. Li, R. Li, H. Zhang, P. Kaghazchi, T. K. Sham, X. Sun, *Adv. Mater.* **2019**, *31*, 1901220; e) L. Luo, S.-H. Chung, A. Manthiram, *Adv. Energy Mater.* **2018**, *8*, 1801014; f) Y. Chen, H. Zhang, W. Xu, X. Yang, Y. Yu, X. Li, H. Zhang, *Adv. Funct. Mater.* **2018**, *28*, 1704987.

[2] a) X. B. Cheng, R. Zhang, C. Z. Zhao, Q. Zhang, *Chem. Rev.* **2017**, *117*, 10403; b) A. Wang, X. Zhang, Y.-W. Yang, J. Huang, X. Liu, J. Luo, *Chem* **2018**, *4*, 2192; c) D. Zhang, S. Wang, B. Li, Y. Gong, S. Yang, *Adv. Mater.* **2019**, *31*, 1901820; d) K. R. Adair, C. Zhao, M. N. Banis, Y. Zhao, R. Li, M. Cai, X. Sun, *Angew. Chem., Int. Ed.* **2019**, *58*, 15797; e) Y. Chen, Y. Luo, H. Zhang, C. Qu, H. Zhang, X. Li, *Small Methods* **2019**, *3*, 1800551.

[3] a) N. W. Li, Y. X. Yin, C. P. Yang, Y. G. Guo, *Adv. Mater.* **2016**, *28*, 1853; b) Y. Zhao, L. V. Goncharova, A. Lushington, Q. Sun, H. Yadegari, B. Wang, W. Xiao, R. Li, X. Sun, *Adv. Mater.* **2017**, *29*, 1606663; c) K. R. Adair, C. Zhao, M. N. Banis, Y. Zhao, R. Li, M. Cai, X. Sun, *Angew. Chem., Int. Ed.* **2019**, *58*, 15797.

[4] a) F. Wu, J. Qian, R. Chen, J. Lu, L. Li, H. Wu, J. Chen, T. Zhao, Y. Ye, K. Amine, *ACS Appl. Mater. Interfaces* **2014**, *6*, 15542; b) J.-S. Kim, T. H. Hwang, B. G. Kim, J. Min, J. W. Choi, *Adv. Funct. Mater.* **2014**, *24*, 5359; c) S. Liu, G. R. Li, X. P. Gao, *ACS Appl. Mater. Interfaces* **2016**, *8*, 7783.

[5] a) K. Yan, Z. Lu, H.-W. Lee, F. Xiong, P.-C. Hsu, Y. Li, J. Zhao, S. Chu, Y. Cui, *Nat. Energy* **2016**, *1*, 16010; b) C. Yang, Y. Yao, S. He, H. Xie, E. Hitz, L. Hu, *Adv. Mater.* **2017**, *29*, 1702714.

[6] L. Suo, Y. S. Hu, H. Li, M. Armand, L. Chen, *Nat. Commun.* **2013**, *4*, 1481.

[7] Y. Zhang, J. Qian, W. Xu, S. M. Russell, X. Chen, E. Nasybulin, P. Bhattacharya, M. H. Engelhard, D. Mei, R. Cao, F. Ding, A. V. Cresce, K. Xu, J. G. Zhang, *Nano Lett.* **2014**, *14*, 6889.

[8] X.-Q. Zhang, X. Chen, X. Xu, J.-Q. Huang, Q. Zhang, *Angew. Chem., Int. Ed.* **2017**, *56*, 14207.

[9] a) C. Z. Zhao, X. Q. Zhang, X. B. Cheng, R. Zhang, R. Xu, P. Y. Chen, H. J. Peng, J. Q. Huang, Q. Zhang, *Proc. Natl. Acad. Sci. USA* **2017**, *114*, 11069; b) D. Lin, P. Y. Yuen, Y. Liu, W. Liu, N. Liu, R. H. Dauskardt, Y. Cui, *Adv. Mater.* **2018**, *30*, 1802661; c) X. Han,

**ADVANCED
SCIENCE NEWS**
www.advancedsciencenews.com

**ADVANCED
ENERGY
MATERIALS**
www.advenergymat.de

Y. Gong, K. K. Fu, X. He, G. T. Hitz, J. Dai, A. Pearse, B. Liu, H. Wang, G. Rubloff, Y. Mo, V. Thangadurai, E. D. Wachsman, L. Hu, *Nat. Mater.* **2017**, *16*, 572; d) X. Yang, Q. Sun, C. Zhao, X. Gao, K. R. Adair, Y. Liu, J. Luo, X. Lin, J. Liang, H. Huang, L. Zhang, R. Yang, S. Lu, R. Li, X. Sun, *Nano Energy* **2019**, *61*, 567.

[10] a) D. Lin, Y. Liu, Z. Liang, H. W. Lee, J. Sun, H. Wang, K. Yan, J. Xie, Y. Cui, *Nat. Nanotechnol.* **2016**, *11*, 626; b) Z. Liang, D. Lin, J. Zhao, Z. Lu, Y. Liu, C. Liu, Y. Lu, H. Wang, K. Yan, X. Tao, Y. Cui, *Proc. Natl. Acad. Sci. USA* **2016**, *113*, 2862; c) K. R. Adair, M. Iqbal, C. Wang, Y. Zhao, M. N. Banis, R. Li, L. Zhang, R. Yang, S. Lu, X. Sun, *Nano Energy* **2018**, *54*, 375; d) X. B. Cheng, T. Z. Hou, R. Zhang, H. J. Peng, C. Z. Zhao, J. Q. Huang, Q. Zhang, *Adv. Mater.* **2016**, *28*, 2888; e) Q. Li, S. Zhu, Y. Lu, *Adv. Funct. Mater.* **2017**, *27*, 1606422.

[11] Z. Liang, K. Yan, G. Zhou, A. Pei, J. Zhao, Y. Sun, J. Xie, Y. Li, F. Shi, Y. Liu, *Sci. Adv.* **2019**, *5*, eaau5655.

[12] Y. Chen, M. Yue, C. Liu, H. Zhang, Y. Yu, X. Li, H. Zhang, *Adv. Funct. Mater.* **2019**, *29*, 1806752.

[13] a) Y. Zhang, W. Luo, C. Wang, Y. Li, C. Chen, J. Song, J. Dai, E. M. Hitz, S. Xu, C. Yang, Y. Wang, L. Hu, *Proc. Natl. Acad. Sci. USA*

2017, *114*, 3584; b) C. Sun, Y. Li, J. Jin, J. Yang, Z. Wen, *J. Mater. Chem. A* **2019**, *7*, 7752.

[14] a) A. Ambrosi, M. Pumera, *Chem. Soc. Rev.* **2016**, *45*, 2740; b) K.-H. Choi, J. Yoo, C. K. Lee, S.-Y. Lee, *Energy Environ. Sci.* **2016**, *9*, 2812; c) K. Sun, T. S. Wei, B. Y. Ahn, J. Y. Seo, S. J. Dillon, J. A. Lewis, *Adv. Mater.* **2013**, *25*, 4539.

[15] a) X. Gao, X. Yang, Q. Sun, J. Luo, J. Liang, W. Li, J. Wang, S. Wang, M. Li, R. Li, T.-K. Sham, X. Sun, *Energy Storage Mater.* **2019**, *1008*, 1001. b) Y. Yu, H. Zhang, X. Yang, J. Gou, X. Tong, X. Li, H. Zhang, *Energy Storage Mater.* **2019**, *19*, 88.

[16] a) Z. Liang, K. Yan, G. Zhou, A. Pei, J. Zhao, Y. Sun, J. Xie, Y. Li, F. Shi, Y. Liu, D. Lin, K. L. H. Wang, H. Wang, Y. Lu, Y. Cui, *Sci. Adv.* **2019**, *5*, eaau5655; b) W. Liu, D. Lin, A. Pei, Y. Cui, *J. Am. Chem. Soc.* **2016**, *138*, 15443.

[17] a) X. Gao, X. Yang, M. Li, Q. Sun, J. Liang, J. Luo, J. Wang, W. Li, J. Liang, Y. Liu, *Adv. Funct. Mater.* **2019**, *29*, 1806724; b) A. Eftekhari, *Sustainable Energy Fuels*, **2017**, *1*, 2053; c) Y. Zhao, M. Amirmaleki, Q. Sun, C. Zhao, A. Codirenzi, L. V. Goncharova, C. Wang, K. Adair, X. Li, X. Yang, *Matter* **2019**, *1*, 1215; d) Y. Wang, Y. Yu, Y. Tan, T. Li, Y. Chen, S. Wang, K. Sui, H. Zhang, Y. Luo, X. Li, *Adv. Energy Mater.* **2019**, 1903233.